Nano Research 2018, 11(9): 4728–4734
https://doi.org/10.1007/s12274-018-2057-1
Research Article
ISSN 1998-0124
CN 11-5974/O4

MoP nanoparticles with a P-rich outermost atomic layer embedded in N-doped porous carbon nanofibers: Self-supported electrodes for efficient hydrogen generation

Minqiang Wang[1], Cui Ye[2], Maowen Xu[1], and Shujuan Bao[1] (✉)

[1] *Institute for Clean Energy & Advanced Materials, Faculty of Materials and Energy, Southwest University, Chongqing 400715, China*
[2] *Key Laboratory of Eco-Environments in Three Gorges Reservoir Region (Ministry of Education), School of Chemistry and Chemical Engineering, Southwest University, Chongqing 400715, China*

Received: 6 January 2018
Revised: 13 March 2018
Accepted: 18 March 2018

KEYWORDS
P-rich outermost atomic layer,
molybdenum phosphide,
density function theory,
self-supported electrocatalyst,
hydrogen evolution reaction

ABSTRACT

Despite being pursued for a long time, hydrogen production via water splitting is still a huge challenge mainly due to a lack of durable and efficient catalysts. Molybdenum phosphide (MoP) is theoretically capable of efficient hydrogen evolution reaction (HER) catalysis, however, there is still room for further improvement in its performance. Herein, we propose a design for MoP with a P-rich outermost atomic layer for enhancing HER via complementary theoretical and experimental validation. The correlation of computational results suggests that the P-terminated surface of MoP plays a crucial role in determining its high-efficiency catalytic properties. We fabricated a P-rich outermost atomic layer of MoP nanoparticles by using N-doped porous carbon (MoP@NPCNFs) to capture more P on the surface of MoP and limit the growth of nanoparticles. Further, the as-prepared material can be directly employed as a self-supported electrocatalyst, and it exhibits remarkable electrocatalytic activity for HER in acidic media; it also reveals excellent long-term durability for up to 5,000 cycles with negligible loss of catalytic activity.

1 Introduction

With the rapid unsustainable consumption of fossil energy, exploiting environmentally friendly renewable energy sources becomes imperative [1–5]. Hydrogen (H_2) production from the electrochemical splitting of water has been extensively studied as a promising solution to the depletion of nonrenewable fossil fuels [6–9]. While Pt-group metals and Pt-based materials have been recognized as state-of-the-art hydrogen evolution reaction (HER) catalysts because of their low onset potentials and Tafel slopes, their high cost and relative scarcity limit their extensive and practical application in HER [10–15]. It is thus highly imperative

Address correspondence to baoshj@swu.edu.cn

to develop high-performance HER electrocatalysts from earth-abundant, low cost elements.

As a result of a similar electronic structure to platinum-group metals, molybdenum phosphide (MoP) has been intensively investigated for its excellent catalytic activities [16, 17]. Amorphous MoP nanoparticles have been synthesized by Schaak et al. and used as an electrocatalyst for HER in acidic aqueous solutions [18]. Wang et al. reported that even the bulk form of MoP exhibits high HER catalytic activity in both acidic and alkaline conditions [19]. As a class of new emerging materials, even in the amorphous structure or bulk form, MoP could display significant catalytic performance for the HER. In addition, recent research has indicated that electrocatalytic activities of catalysts strongly depend on their surface atomic structures [20]. For example, the adsorption of atomic hydrogen is desirable on the P-rich surface of Rh_2P, and leads to a high catalytic activity in HER, indicating that the adsorption energies of reactive intermediates could be optimized [21]. Beyond this, there is still room for further improvement of the performance of MoP by controlling the specific nanostructure, reducing the size of nanoparticles (NPs), and/or adjusting the surface atomic structure. Phase-forming of MoP generally occurs at high temperatures, thus agglomeration is inevitable during sintering [22]. It is therefore still a challenge to fabricate well-crystallized MoP nanostructures and expose sufficient active sites to enhance HER performance.

In this study, MoP was selected as a model cathode material to comprehensively investigate the effect of a terminated surface for HER by complementary theoretical and experimental approaches. As a preliminary trial, density function theory (DFT) calculations validated that a P-terminated MoP(001) surface is more stable than a Mo-terminated surface in the whole range of phosphorus chemical potentials from P-poor to P-rich boundaries. This indicates that the P-terminated surface plays a crucial role in determining its high-efficiency catalyst properties, and P-terminated MoP(001) shows outstanding catalytic activity for HER under high coverage of hydrogen. We designed an efficient strategy to construct a P-rich outermost atomic layer in MoP nanoparticles for the first time. In our experiments, Mo cations and phosphate anions were dispersed in a polyacrylonitrile (PAN) solution at an atomic level and embedded into electrospun PAN to form composite nanofibers. Further, with a controlled pyrolysis reduction treatment, phosphate was transformed into phosphide nanoparticles, and the primary PAN was carbonized to carbonaceous residues. The accompanying N-doped porous carbon provides rich electron lone pairs to capture P during the reduction of metal orthophosphates, and to construct MoP with a P-rich outermost atomic layer. At the same time, the high porosity developed during pyrolysis can be used as a molecular sieve to host *in situ* the generated phosphide nanocrystals. Annular dark-field scanning transmission electron microscopy (ADF-STEM) shows that MoP nanoparticles with a P-rich outermost atomic layer were successfully constructed. Electrochemical tests show that this MoP with a P-rich outermost atomic layer displays prominent HER activity. Carbon coating protects the phosphide nanoparticles from oxidation, giving them long-term durability under HER operation conditions. In addition, the unique MoP nanoparticles embedded N-doped porous carbon nanofiber (MoP-NPCNF) catalyst system can be directly used as an electrode for HER, and it displays excellent stability.

2 Results and discussion

A detailed analysis of the microscopic structure near the surface is critical in revealing the reasons for the excellent performance of MoP as a catalyst. For one MoP with surface enclosed by facet, Mo or P will be the exclusive termination atom. Initially, the stable surface of MoP (001) was calculated using DFT, as shown in Fig. 1(a). The results show that a P-terminated (Fig. 1(c)) MoP (001) surface is more stable than a Mo-terminated (Fig. 1(b)) surface in the range of P chemical potentials from P-poor to P-rich boundaries, which indicates that the most active sites are likely found on a P-terminated surface. These results are consistent with the previous calculations [21].

The HER activity can be described well by the adsorption free energy of *H on catalysts [23–25]. Furthermore, the free energy of *H can be calculated to evaluate the catalytic activity of MoP. The ΔG_H of the P-terminated (solid line) and Mo-terminated

(dotted line) surfaces with different H coverage were investigated, as shown in Fig. 2. The Mo atoms in the Mo-terminated surface exhibit strong binding to hydrogen atoms, indicating that Mo is not likely to be the active site. However, P-terminated MoP presents a free energy for *H that is smaller by 0.2 eV at higher coverages (1 monolayer (ML)), indicating the importance of P atoms to hydrogen evolution. In short, our calculations indicate that, for MoP as a catalyst, P-terminated MoP (001) shows outstanding catalytic activity for HER under high coverage of H.

To validate the above theoretical analysis, MoP with a P-rich outermost atomic layer was successfully embedded in N-doped porous carbon nanofibers by electrospinning. In this work, PAN, a promising engineering polymer with excellent mechanical and thermal properties, was used to produce homogeneous nanofiber-based large-scale films. After further heating the precursor in a H_2 atmosphere, the organic ligands in the PAN molecules decompose and are converted into N-doped porous carbon materials. Meanwhile, molybdate salt and phosphoric acid, serving as Mo and P sources, respectively, are reduced to MoP with a P-rich outermost atomic layer, which is also limited in terms of the ultrafine porosity residues accompanying the decomposition of PAN. This phase MoP@NPCNFs was structurally characterized by X-ray diffraction (XRD), as shown in Fig. 3(a). The diffraction peaks of the as-prepared MoP@NPCNFs indicate that it consists of hexagonal MoP with lattice parameters $a = b =$ 3.222 Å and c = 3.191 Å (JCPDS: 89-5110). The broad peak around 24° is ascribed to hexagonal graphite. No other impurity peaks are observed, indicating the sample is of high purity. The microstructure of the precursors and pyrolyzed product were first characterized by field-emission scanning electron microscopy (FESEM). Figure S1(a) in the Electronic Supplementary Material (ESM) displays a typical FESEM image of the precursors, revealing a flexible cloth-like architecture. The high-resolution FESEM image of the precursor in Fig. S1(b) in the ESM shows a smooth and uniform solid one-dimensional (1D) nanofiber structure several micrometers long. As expected, the resulting MoP@NPCNFs (Fig. 3(b)) retain the cloth-like architecture and pristine fibroid morphology of the precursors even after high-temperature pyrolysis. Benefiting from an entangled network, the obtained MoP@NPCNFs exhibit high flexibility (inset of Fig. 3(b)). The high-resolution FESEM image in Fig. 3(c) clearly displays nanofibers with an average diameter of 200 nm, and roughened surfaces. Figures 3(d) and 3(e) show the representative bright-field and dark-field transmission electron microscopy (TEM) images of MoP@NPCNFs, respectively, in which nanofibers can be observed. The dispersed ultrafine MoP nanoparticles are bunched near the porous N-doped carbon nanofibers. Such a configuration not only prevents the growth and aggregation of the nanocrystals but also benefits electronic and ionic transfer. Based on the high- resolution TEM (HRTEM) image, the lattice fringes of the ultrafine nanoparticles are 0.32 nm in size, consistent with the (001) plane of MoP. The surface of the nanoparticle is covered by graphitic carbon with 0.36 nm lattice spacing of the (002) plane, indicating high crystallinity of the prepared sample. High-angle annular dark-field scanning transmission electron microscopy-energy-dispersive X-ray spectroscopy (HAADF-STEM-EDS) elemental

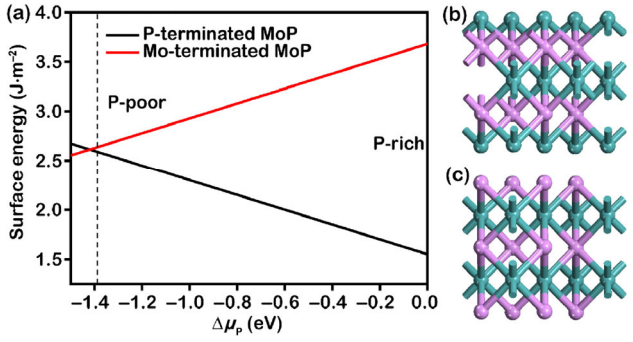

Figure 1 (a) Surface energy of the MoP (001) surface. The P-terminated and Mo-terminated MoP (001) are indicated by the black and red lines, respectively. (b) and (c) Schematic diagrams of the Mo-terminated and P-terminated surfaces, respectively. The green spheres indicate Mo atom, and magenta spheres P atoms.

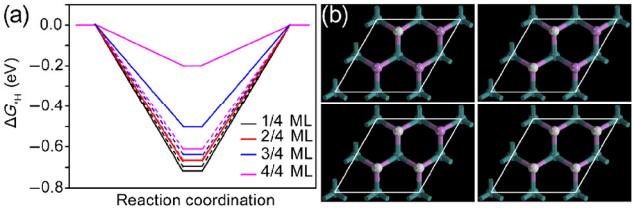

Figure 2 (a) Calculated adsorption free energy of H for P-terminated (solid line) and Mo-terminated (dotted line) MoP for different coverages. (b) Optimized structures of H adsorption for different coverages on the P-terminated surface.

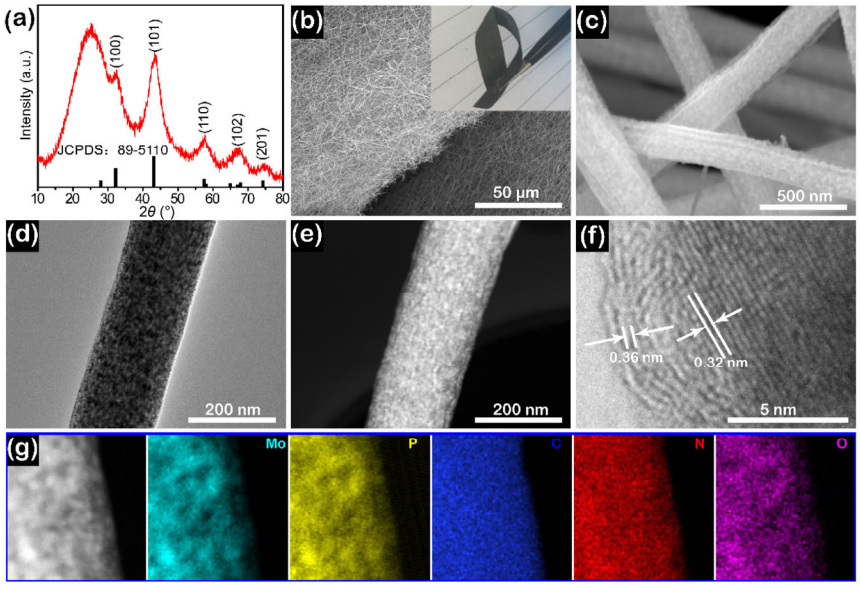

Figure 3 (a) Experimental and simulated XRD patterns of as-prepared MoP@NPCNFs, (b) low-resolution FESEM image, (c) high-resolution FESEM image, (d) TEM image, (e) STEM image and (f) HRTEM image of the MoP@NPCNFs. Inset in (b) is the corresponding optical photograph of flexible MoP@NPCNFs. (g) Large area STEM-EDS element mapping images of the MoP@NPCNFs nanocrystal.

mapping images in Fig. 3(g) and Fig. S2 in the ESM suggest homogeneous distribution of all the elements Mo, P, C, N, and O. The chemical composition was further elucidated by X-ray photoelectron spectroscopy (XPS) (Figs. S3 and S4 in the ESM), indicating the existence of Mo, P, C, N, and O in the sample. The atomic ratio of Mo to P is about 1:1, further corroborating that MoP crystals were successfully prepared.

Along with a controllable pyrolysis reduction treatment, the accompanying N-doped porous carbon provides electron-rich lone pairs to capture P during the reduction of metal orthophosphates, and further synthesize MoP with a P-rich outermost atomic layer. ADF-STEM allows us to evaluate the atomic structures of the MoP nanoparticles. An ADF-STEM image (Fig. 4(a)) and high-resolution ADF-STEM images (Figs. 4(b) and 4(c)) show the structure of the nanoparticle near the surface in the (001) orientation. Clearly, the outermost atomic layer appears darker than the layer underneath. Based on the contrast in ADF-STEM, approximately scaled with $Z^{1.7}$, the result strongly supports the identification of the surface atoms as P atoms.

Our DFT calculation results indicate that the efficient catalytic activity of MoP for HER is derived from

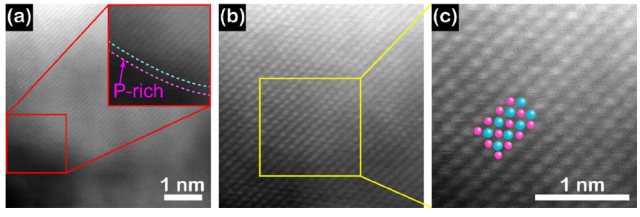

Figure 4 (a) ADF-STEM image of a part of one MoP nanoparticle. The inset in (a) shows that the outermost surface is P-rich. (b) and (c) High-resolution ADF-STEM images of MoP with the corresponding crystal structure superimposed.

the P atoms due to the very small value of ΔG_H. To further evaluate the important role of P atoms, high-resolution XPS of Mo 3d and P 2p were carried out to characterize the electron transfer from Mo to P. As shown in Fig. S5 in the ESM, doublets at 235.86 eV/231.88 eV (Mo $3d_{3/2}$) can be ascribed to the oxidation state of Mo, and another doublet at 232.91 eV/228.3 eV (Mo $3d_{5/2}$) can be ascribed to MoP, which shows a small Mo $3d_{5/2}$ peak at 228.3 eV located at a slightly higher binding energy than that assigned to metallic Mo (Mo0 227.4–224.8 eV) [26], indicating that Mo in MoP@NPCNFs bears a partial positive charge (δ^+). In addition, P $2p_{3/2}$ with a binding energy of 129.4 eV is negatively shifted from that of P^0, which suggests that P has a slight negative charge (δ^-). These results indicate a weak electron density transfer from Mo to

P in MoP@NPCNFs. As a result, the binding energy with *H is neither too weak nor too strong, and further benefits the electrochemical HER process.

Based on the above results, this unique nanostructure of MoP@NPCNFs appears to be a new, innovative method to fabricate a HER catalyst. Subsequently, we compared the electrochemical catalytic activity of NPCNFs (Fig. S6 in the ESM), MoP@NPCNFs, MoP nanofibers (MoP NFs) (Fig. S7 in the ESM), and commercial Pt/C using a standard three-electrode electrochemical cell in acid conditions. A flexible film of MoP@NPCNFs was used as the working electrode, and the current used for NPCNFs, MoP NFs, and Pt/C was normalized to a carbon cloth with the same geometric area as MoP@NPCNFs. As shown in Fig. 5(a), at a current density of 10 mA·cm^{-2}, the NPCNFs displayed negligible HER activity; however, MoP@NPCNFs exhibited an overpotential of 64 mV, lower than that of pure MoP NFs (96 mV), whereas a commercial Pt/C electrode shows the highest HER activity with a near-zero onset overpotential. To further study the HER activity, Tafel slopes were calculated from the polarization curves for MoP@NPCNFs, MoP NFs, and commercial Pt/C to be 65.64, 73.28, and 41.65 mV·dec^{-1} (Fig. 5(b)), respectively. Benefiting from its unique nanostructure, the MoP@NPCNFs exhibits efficient HER activity, close to that of commercial Pt/C.

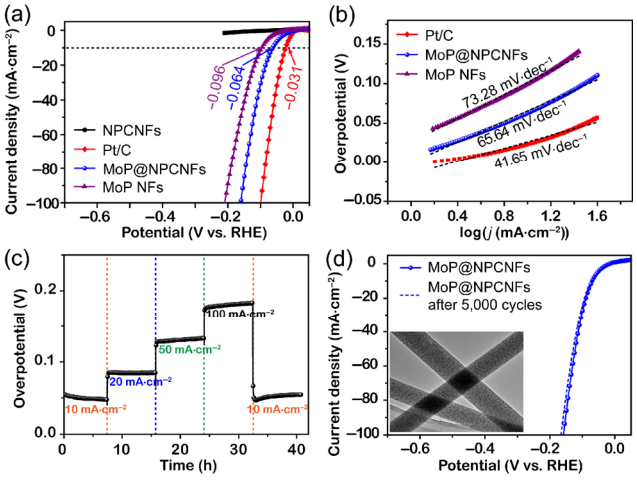

Figure 5 (a) Polarization curves of NPCNFs, Pt/C, MoP@NPCNFs, and MoP NFs at 5 mV·s^{-1} in 0.5 M H_2SO_4. (b) The corresponding Tafel slopes of Pt/C, MoP@NPCNFs, and MoP NFs. (c) Multicurrent process of MoP@NPCNFs investigated at different current densities and times. (d) Polarization curves for MoP@NPCNFs before and after 5,000 cycles of CV scanning.

Therefore, the HER overpotential and Tafel slope of MoP@NPCNFs are lower than most recent reported TMPs, such as CoP/carbon nanotubes (165 mV and 68 mV·dec^{-1}) [27], Cu_3P nanowire arrays (143 mV and 67 mV·dec^{-1}) [28], WP nanorod arrays (130 mV and 69 mV·dec^{-1}) [29], Ni_5P_4-Ni_2P (120 mV and 79.1 mV·dec^{-1}) [30], and the other reported highly active HER electrocatalysts that are listed in Table S1 in the ESM. There is an observed improvement compared to the previously reported MoP@porous carbon [16], which displays an impressive overpotential of 153 mV and a Tafel slope of 66 mV·dec^{-1} despite the high resistivity of porous carbon, suggesting an intrinsically high HER catalytic activity of the MoP@NPCNFs with a P-rich outermost atomic layer. A fast charge transfer is also indicated by the electrochemical impedance spectra (EIS) shown in Fig. S8 in the ESM (at η = 100 mV). As expected, the MoP-NPCNFs composite catalyst exhibits much lower charge transfer resistance than the pure MoP NFs.

To evaluate the electrochemical surface area of the catalysts, the electrochemical double layer capacitance (Cdl) was surveyed by a simple cyclic voltammetry (CV) test (Fig. S9 in the ESM). It is worthwhile mentioning that the Cdl of MoP@NPCNFs was 43.46 mF·cm^{-2}, which is approximately three times higher than that of MoN NFs (13.04 mF·cm^{-2}) and ten times that of bulk MoN (4.27 mF·cm^{-2}), suggesting that the structure of MoP@NPCNFs is unique; this allows the maximum exposure of the active sites that further enhances the HER activity.

The long-term durability of MoP@NPCNFs was tested by applying a continuous current without any activation at 10, 20, 50, and 100 mA·cm^{-2}. Even at 50 and 100 mA·cm^{-2}, the potential was still well maintained. Clearly, MoP@NPCNFs is very stable. After 32 h HER, the current density returned to 10 mA·cm^{-2}, and the corresponding potential was consistent with the initial value, demonstrating its outstanding durability. The excellent long-term durability was also corroborated by the CV scans. After 5,000 continuous cycles of CV scanning, the polarization curve of the MoP@NPCNFs shows almost negligible degradation (Fig. 5(d)), and the microstructure after 5,000 cycles is hardly altered (inset of Fig. 5(d)), further indicating optimal HER stability.

3 Conclusions

In summary, a concept of MoP with a P-rich outermost atomic layer with outstanding catalytic activity for HER performance is proposed, and supported by theoretical calculations. Followed by experimental validation, we developed a design and constructed MoP nanoparticles with a P-rich outermost atomic layer embedded in porous N-doped carbon nanofibers, in which highly dispersed MoP nanoparticles are deposited in the porous N-doped carbon nanofibers without aggregation. Using this general strategy, we demonstrated that this composite exhibits remarkable electrocatalytic activity, close to that of the Pt/C catalyst for HER in acidic media, and excellent long-term durability for up to 5,000 cycles with negligible catalytic activity loss. Based on these results, this strategy opens a new avenue for the construction of phosphide catalysts with P-rich outermost atomic layers for next-generation sustainable electrochemical water splitting.

Acknowledgements

This work is financially supported by the National Natural Science Foundation of China (No. 21773188), Fundamental Research Funds for the Central Universities (Nos. XDJK2017D003 and XDJK2017B055), Program for Excellent Talents in Chongqing (No. 102060-20600218), and Program for Innovation Team Building at Institutions of Higher Education in Chongqing (No. CXTDX201601011) and Chongqing Key Laboratory for Advanced Materials and Technologies.

Electronic Supplementary Material: Supplementary material (sample preparation procedure; FESEM images of the precursors, NPCNFs, and MoP NFs; EDS spectrum of MoP@NPCNFs; XPS survey scan of MoP@NPCNFs; Nyquist plots of NPCNFs, MoP@NPCNFs, and MoP NFs) is available in the online version of this article at https://doi.org/10.1007/s12274-018-2057-1.

References

[1] Fan, J. C.; Qi, K.; Zhang, L.; Zhang, H. Y.; Yu, S. S.; Cui, X. Q. Engineering Pt/Pd interfacial electronic structures for highly efficient hydrogen evolution and alcohol oxidation. *ACS Appl. Mater. Interfaces* **2017**, *9*, 18008–18014.

[2] Liao, H. B.; Wei, C.; Wang, J. X.; Fisher, A.; Sritharan, T.; Feng, Z. X.; Xu, Z. J. A multisite strategy for enhancing the hydrogen evolution reaction on a nano-Pd surface in alkaline media. *Adv. Energy Mater.* **2017**, *7*, 1701129.

[3] Voiry, D.; Salehi, M.; Silva, R.; Fujita, T.; Chen, M. W.; Asefa, T.; Shenoy, V. B.; Eda, G.; Chhowalla, M. Conducting MoS_2 nanosheets as catalysts for hydrogen evolution reaction. *Nano Lett.* **2013**, *13*, 6222–6227.

[4] Ye, G. L.; Gong, Y. J.; Lin, J. H.; Li, B.; He, Y. M.; Pantelides, S. T.; Zhou, W.; Vajtai, R.; Ajayan, P. M. Defects engineered monolayer MoS_2 for improved hydrogen evolution reaction. *Nano Lett.* **2016**, *16*, 1097–1103.

[5] Zhou, W. J.; Jia, J.; Lu, J.; Yang, L. J.; Hou, D. M.; Li, G. Q.; Chen, S. W. Recent developments of carbon-based electrocatalysts for hydrogen evolution reaction. *Nano Energy* **2016**, *28*, 29–43.

[6] Tian, L. H.; Yan, X. D.; Chen, X. B. Electrochemical activity of iron phosphide nanoparticles in hydrogen evolution reaction. *ACS Catal.* **2016**, *6*, 5441–5448.

[7] Popczun, E. J.; Read, C. G.; Roske, C. W.; Lewis, N. S.; Schaak, R. E. Highly active electrocatalysis of the hydrogen evolution reaction by cobalt phosphide nanoparticles. *Angew. Chem., Int. Ed.* **2014**, *53*, 5427–5430.

[8] Popczun, E. J.; McKone, J. R.; Read, C. G.; Biacchi, A. J.; Wiltrout, A. M.; Lewis, N. S.; Schaak, R. E. Nanostructured nickel phosphide as an electrocatalyst for the hydrogen evolution reaction. *J. Am. Chem. Soc.* **2013**, *135*, 9267–9270.

[9] Yu, J. Y.; Zhou, W. J.; Xiong, T. L.; Wang, A. L.; Chen, S. W.; Chu, B. L. Enhanced electrocatalytic activity of Co@N-doped carbon nanotubes by ultrasmall defect-rich TiO_2 nanoparticles for hydrogen evolution reaction. *Nano Res.* **2017**, *10*, 2599–2609.

[10] Liao, L.; Wang, S. N.; Xiao, J. J.; Bian, X. J.; Zhang, Y. H.; Scanlon, M. D.; Hu, X. L.; Tang, Y.; Liu, B. H.; Girault, H. H. A nanoporous molybdenum carbide nanowire as an electrocatalyst for hydrogen evolution reaction. *Energy Environ. Sci.* **2014**, *7*, 387–392.

[11] Cheng, L.; Huang, W. J.; Gong, Q. F.; Liu, C. H.; Liu, Z.; Li, Y. G.; Dai, H. J. Ultrathin WS_2 nanoflakes as a high-performance electrocatalyst for the hydrogen evolution reaction. *Angew. Chem., Int. Ed.* **2014**, *53*, 7860–7863.

[12] Callejas, J. F.; Read, C. G.; Popczun, E. J.; McEnaney, J. M.; Schaak, R. E. Nanostructured Co_2P electrocatalyst for the hydrogen evolution reaction and direct comparison with morphologically equivalent CoP. *Chem. Mater.* **2015**, *27*, 3769–3774.

[13] Li, Y. J.; Zhang, H. C.; Jiang, M.; Kuang, Y.; Sun, X. M.; Duan, X. Ternary NiCoP nanosheet arrays: An excellent bifunctional catalyst for alkaline overall water splitting. *Nano Res.* **2016**, *9*, 2251–2259.

[14] Wang, M. Q.; Ye, C.; Liu, H.; Xu, M. W.; Bao, S. J. Nanosized metal phosphides embedded in nitrogen-doped porous carbon nanofibers for enhanced hydrogen evolution at all pH values. *Angew. Chem., Int. Ed.* **2018**, *57*, 1963–1967.

[15] Wang, M. Q.; Ye, C.; Bao, S. J.; Chen, Z. Y.; Liu, H.; Xu, M. W. Ternary $Ni_xCo_{3-x}S_4$ with fine hollow nanostructure as robust electrocatalyst for hydrogen evolution. *ChemCatChem* **2017**, *9*, 4169–4174.

[16] Yang, J.; Zhang, F. J.; Wang, X.; He, D. S.; Wu, G.; Yang, Q. H.; Hong, X.; Wu, Y.; Li, Y. D. Porous molybdenum phosphide nano-octahedrons derived from confined phosphorization in UIO-66 for efficient hydrogen evolution. *Angew. Chem., Int. Ed.* **2016**, *55*, 12854–12858.

[17] Jia, J.; Zhou, W. J.; Li, G. X.; Yang, L. J.; Wei, Z. Q.; Cao, L. D.; Wu, Y. S.; Zhou, K.; Chen, S. W. Regulated synthesis of Mo sheets and their derivative MoX sheets (X: P, S, or C) as efficient electrocatalysts for hydrogen evolution reaction. *ACS Appl. Mater. Interfaces* **2017**, *9*, 8041–8046.

[18] McEnaney, J. M.; Crompton, J. C.; Callejas, J. F.; Popczun, E. J.; Biacchi, A. J.; Lewis, N. S.; Schaak, R. E. Amorphous molybdenum phosphide nanoparticles for electrocatalytic hydrogen evolution. *Chem. Mater.* **2014**, *26*, 4826–4831.

[19] Xiao, P.; Sk, M. A.; Thia, L.; Ge, X. M.; Lim, R. J.; Wang, J. Y.; Lim, K. H.; Wang, X. Molybdenum phosphide as an efficient electrocatalyst for the hydrogen evolution reaction. *Energy Environ. Sci.* **2014**, *7*, 2624–2629.

[20] Li, F.; Zhao, X. L.; Mahmood, J.; Okyay, M. S.; Jung, S. M.; Ahmad, I.; Kim, S. J.; Han, G. F.; Park, N.; Baek, J. B. Macroporous inverse opal-like Mo_xC with incorporated Mo vacancies for significantly enhanced hydrogen evolution. *ACS Nano* **2017**, *11*, 7527–7533.

[21] Duan, H. H.; Li, D. G.; Tang, Y.; He, Y.; Ji, S. F.; Wang, R. Y.; Lv, H. F.; Lopes, P. P.; Paulikas, A. P.; Li, H. Y. et al. High performance Rh_2P electrocatalyst for efficient water splitting. *J. Am. Chem. Soc.* **2017**, *139*, 5494–5502.

[22] Xing, Z. C.; Liu, Q.; Asiri, A. M.; Sun, X. P. Closely interconnected network of molybdenum phosphide nanoparticles: A highly efficient electrocatalyst for generating hydrogen from water. *Adv. Mater.* **2014**, *26*, 5702–5707.

[23] Liu, Y. P.; Yu, G. T.; Li, G. D.; Sun, Y. H.; Asefa, T.; Chen, W.; Zou, X. X. Coupling Mo_2C with nitrogen-rich nanocarbon leads to efficient hydrogen-evolution electrocatalytic sites. *Angew. Chem., Int. Ed.* **2015**, *54*, 10752–10757.

[24] Hinnemann, B.; Moses, P. G.; Bonde, J.; Jørgensen, K. P.; Nielsen, J. H.; Horch, S.; Chorkendorff, I.; Nørskov, J. K. Biomimetic hydrogen evolution: MoS_2 nanoparticles as catalyst for hydrogen evolution. *J. Am. Chem. Soc.* **2005**, *127*, 5308–5309.

[25] Skúlason, E.; Tripkovic, V.; Björketun, M. E.; Gudmundsdóttir, S.; Karlberg, G.; Rossmeisl, J.; Bligaard, T.; Jónsson, H.; Nørskov, J. K. Modeling the electrochemical hydrogen oxidation and evolution reactions on the basis of density functional theory calculations. *J. Phys. Chem. C* **2010**, *114*, 18182–18197.

[26] Phillips, D. C.; Sawhill, S. J.; Self, R.; Bussell, M. E. Synthesis, characterization, and hydrodesulfurization properties of silica-supported molybdenum phosphide catalysts. *J. Catal.* **2002**, *207*, 266–273.

[27] Pan, Y.; Lin, Y.; Chen, Y. J.; Liu, Y. Q.; Liu, C. G. Cobalt phosphide-based electrocatalysts: Synthesis and phase catalytic activity comparison for hydrogen evolution. *J. Mater. Chem. A* **2016**, *4*, 4745–4754.

[28] Tian, J. Q.; Liu, Q.; Cheng, N. Y.; Asiri, A. M.; Sun, X. P. Self-supported Cu_3P nanowire arrays as an integrated high-performance three-dimensional cathode for generating hydrogen from water. *Angew. Chem., Int. Ed.* **2014**, *53*, 9577–9581.

[29] Pu, Z. H.; Liu, Q.; Asiri, A. M.; Sun, X. P. Tungsten phosphide nanorod arrays directly grown on carbon cloth: A highly efficient and stable hydrogen evolution cathode at all pH values. *ACS Appl. Mater. Interfaces* **2014**, *6*, 21874–21879.

[30] Wang, X. G.; Kolen'Ko, Y. V.; Bao, X. Q.; Kovnir, K.; Liu, L. F. One-step synthesis of self-supported nickel phosphide nanosheet array cathodes for efficient electrocatalytic hydrogen generation. *Angew. Chem., Int. Ed.* **2015**, *54*, 8188–8192.